Estimation of Drain Pipe Effects Using Electrical Prospecting and Unsaturated Soil/Water Coupled Analysis

K. Kawai[1], K. Nakashima[1], K. Yasutomi[2], and N. Otaka[2]
[1]*Department of Civil and Environmental Engineering, Kindai University, Higashi-Osaka, Japan*
[2]*Products Development Center, Nippon Steel, Tokyo, Japan*
E-mail: kkawai@civileng.kindai.ac.jp

ABSTRACT: Elevation of the phreatic surface causes instability in earth structures. Therefore, drainage systems are important in constructing an earth structure. Drain pipes are a drainage system applicable even for an existing earth structure. However, it is difficult to estimate the effects of the drain pipe quantitatively, and design and construction of the drain pipe is conducted based on past experience. In this study of railway embankment with installed drain pipes, electrical prospecting of the phreatic surface and seepage analysis was conducted. In the seepage analysis, a 'permeable boundary' was newly applied to express the effects of the drain pipe for the existing unsaturated soil/water coupled analysis code. Consequently, the permeable boundary was validated for expressing the effects of the drain pipe. Preliminary seepage analysis on the installed drain pipe enabled us to design the optimum array and/or insertion length of the drain pipes.

KEYWORDS: Drain pipe, Phreatic surface, Electrical prospecting, Unsaturated soil/water coupled analysis.

1. INTRODUCTION

An earth structure, such as an embankment or a cutting, becomes unstable when it contains an increasing amount of water, as its phreatic surface rises because of rainfall or the phreatic surface rises because of a rise in the surrounding area's phreatic level, which supplies water to the earth structure from outside. Therefore, drainage works to discharge seepage water and groundwater. For the most part, drainage measures are planned during design of the structure. To accurately know the amount of seepage water and how the phreatic surface behaves, it is necessary to acquire soil conditions and other detailed information. To meet this need, drainage work that can be applied to existing earth structures and natural slopes is required. Drain pipes are slit steel pipes installed by being directly thrust into the ground. They are intended to guide subsurface water out of the earth structure. They are also expected to strengthen the ground owing to compaction around the drain pipe driven into the ground and constrained local deformation. Accordingly, drain pipes have long been installed as drainage measures for existing structures. Oftentimes, they are used with problematic structures on an as-needed basis, and their effectiveness under specific conditions is verified in individual cases. Consequently, engineers have planned the scope of drainage work, drain pipe arrangement, the lengths of pipe driven into the ground, and other design elements based on past experiences. To quantitatively evaluate the effects of drain pipes, Saito et al. (1968) studied the basic drainage mechanisms of drain pipes by conducting seepage testing using a model soil tank. They also conducted experiments using a large model, carried out field surveys, and reported on the relationship of distances between drain pipes driven into ground and pore water pressure reduction effects. Choi (1984) derived an empirical equation referred to the ground installed drain pipes, which provides the way to calculate the downstream water depth as a function of the drain spacing and slope of the impermeable bed, from a set of laboratory experiments. Regarding the lengths of drain pipes driven into the ground, Fujii et al. (1996) proved that their effectiveness in reducing the pore water pressure reaches a plateau when a certain length is exceeded. Resnick and Znidarčić (1994) conducted centrifugal experiments with model installed drain pipes and verified the published design charts of drain pipe. Singh et al. (2019) also investigated the effects of drain pipes with centrifugal model experiments and showed that drain pipe can restrain not only rise of pore water pressure but also deformation of an earth structure. Moreover, Rahrdjo et al. (2003, 2011) indicated the effectiveness of drain pipes for slope stability through field monitoring. To reveal the effects of drain pipes through a seepage analysis, Cai et al. (1998) expressed the lowering of phreatic surface by entering zero pressure head at nodes at the top of drain pipes. They also reported on changes in safety factors determined by stability calculations using a shear strength reduction method. Ota et al. (2012) compared results from a model experiment with installed drain pipes and a three-dimensional seepage analysis in investigating the application of the skin effect, in which the hydraulic conductivity decreases in proximity to a drain pipe. Using the analysis model used by Ota et al., Watanabe et al. (2015) conducted a seepage analysis of a virtual embankment to study the effects of the length of drain pipe driven into the ground and drain pipe intervals. Kitaguchi et al. (2013) expressed the effects of drain pipes in a seepage analysis, considering the range of the effects of drain pipes and, as a pseudo three-dimensional model, correcting the hydraulic conductivity at drain pipe positions. When planning drain pipes in practice, it is necessary to accurately measure the actual phreatic surface and plan drain pipe installation accordingly.

The present study uses electrical prospecting and performs a seepage analysis on an actual embankment installed with drain pipes with the aim of elucidating the effects of drain pipes on phreatic surface shape and quantifying drainage performance. Additionally, it explores techniques to incorporate these clarified effects into drain pipe arrangement planning.

2. TRACKING DOWN THE PHREATIC SURFACE BY ELECTRICAL PROSPECTING

To verify the effects of drain pipe operation, electrical prospecting was performed on an actual railway embankment installed with drain pipes.

2.1 Electrical Prospecting

Electrical prospecting is a technique for determining the subsurface resistivity distribution from potential responses detected on the ground surface when a direct current is passed through the ground. The technique uses a pair of transmitting electrodes (C_m, C_n) and another pair of receiving electrodes (P_m, P_n) to measure the apparent resistivity of the ground between the receiving electrodes, based on the potential difference between the transmitting electrodes and the potential difference between the receiving electrodes (Figure 1). The term apparent resistivity is used here because the measurement is an average resistivity between electrodes. An inverse analysis after measurement can determine spatial resistivity distribution. Moreover, by densely installing electrodes, resistivity distributions can be obtained with a higher resolution. The arrangement of the four electrodes involves several combinations. Electrical resistivity measurements obtained from the ground vary with many factors associated with the geologic bed, including porosity, water saturation,

and resistivity of pore fluid, clay mineral content, and temperature. Given the same soil, electrical resistivity measurements reflect the product of porosity and water saturation, which equals the distribution of water content by volume (porosity × water saturation = distribution of water content by volume). A multi-channel digital resistivity meter manufactured by Oyo Corporation was utilized to enable fast two-dimensional electrical prospecting by automatically switching between the transmitting and receiving electrodes (Figure 2).

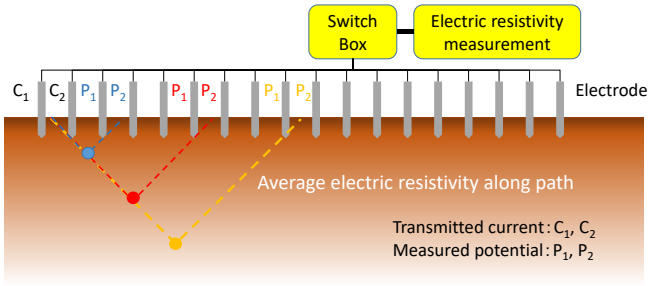

Figure 1 Electrical prospecting overview

Figure 2 Electrical prospecting equipment and operation

2.2 Site Overview and the Results of Electrical Prospecting

Figure 3 shows a schematic diagram of the widened railway embankment and prospecting lines used in this study. Fifteen drain pipes were installed and arranged as three, five-pipe rows, with pipes placed at 2 m intervals as shown in Figure 4. Pipes with varying diameters (three diameters along the length of each pipe) were installed. The pipe was thinner at one end than the other to reduce friction when driven into the ground. Pipes were driven 6 m into the ground. The minimum pipe diameter was 4.9 cm, and the maximum pipe diameter was 7.6 cm. Observation wells were constructed to measure the phreatic level. Pressure-sensitive water level gauges were installed in the wells. The drain pipes were installed in the embankment at locations where the phreatic level was originally high (the embankment had collapsed more than once due to rainfall). Meanwhile, observation well 1 was placed in a location where the phreatic level was low, outside of and merely 10 m away from the drain pipe installation area. This suggests localized presence of groundwater in the embankment.

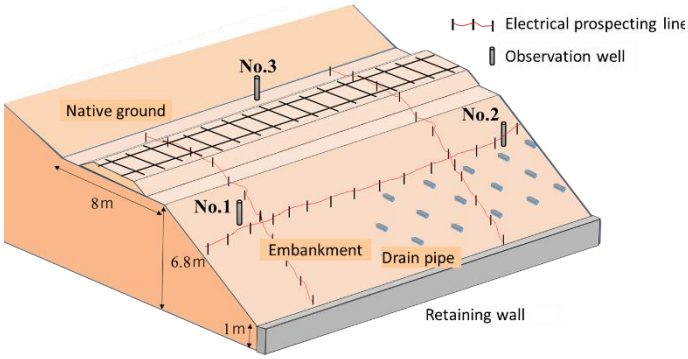

Figure 3 Rough sketch of site and prospecting lines

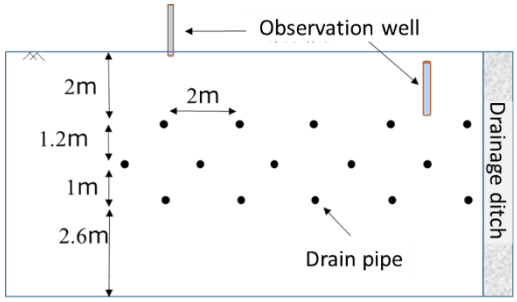

Figure 4 Drain pipe arrangement

Figure 5 plots the relationship between observation well levels and 24-hour effective precipitation at the site after drain pipe installation. The figure also shows, with dashed lines, the levels of observation wells 1, 2, and 3 measured before the drain pipe installation when 24-hour effective precipitation was 188 mm. Observation well 3 in the native ground exhibited no noticeable long-term variation for two years after drain pipe construction. Nonetheless, due to the effect of the drain pipe installation, the average water level decreased by about 60 cm from that observed before construction. The water level of observation well 2, located in the drain pipe installation area, substantially dropped due to the installed drain pipes, and is interpreted to be on a gradually decreasing trend in the long term; although, the level did rise when precipitation occurred. Moreover, when measured during a torrential rain in July 2018, with effective precipitation exceeding 700 mm, the water level remained lower than that observed before drain pipe installation. In observation well 1, outside of the drain pipe installation area, the phreatic level, although in the low-level region, exhibited radical fluctuation in response to rainfall. It is likely that the soil structure in that location drains well. Based on this assumption, electrical prospecting was conducted by placing prospecting lines along a longitudinal section of the embankment crossing observation wells 1 and 2, along a transverse section crossing observation well 1 (not crossing drain pipes), and along a transverse section crossing the canter of the drain pipe installation area, as shown in Figure 3. Along the longitudinal section, electrodes were placed at 80 cm intervals, while along the transverse sections, electrodes were placed at 50 cm intervals on average. This electrical prospecting used a dipole-dipole electrode configuration.

Figures 5, 6, and 7 show electrical resistivity distributions determined for each section based on electrical prospecting performed on December 27, 2019. Although no rain gauge data was obtained at the site, the Meteorological Agency rain gauge, located near the site, was used to compute 24-hour effective precipitation, which during electrical prospecting was 25 to 30 mm. Electrical resistivity was noticeably high in the tracked ballast because of larger pores and a smaller amount of water than in the subgrade. Electrical resistivity was low in the drain pipe installation area (15.0 to 25.0 along the x-axis), as illustrated in the longitudinal section in Figure 6. As stated earlier, electrical resistivity is affected by clay content and other soil qualities, as well as by the amount of water. Although no definite information is available as to what materials were used after past collapses and to what extent collapses were repaired, it is clear that the substantially high-water content necessitated drain pipe installation, as revealed by the phreatic level. Figure 7 presents the section that crossed observation well 1, located away from the drain pipe installation area. The contour diagram indicates water levels in observation wells 1 and 3 measured on the day of electrical prospecting. The white dashed line represents a phreatic surface surmised from observed water levels and electrical resistivity distributions. Bamboo, which loves water, grows on the slope of the embankment. However, no bamboo grew in the 10 m wide zone in which this prospecting line was placed. Given these factors, the results of electrical prospecting should be reliable.

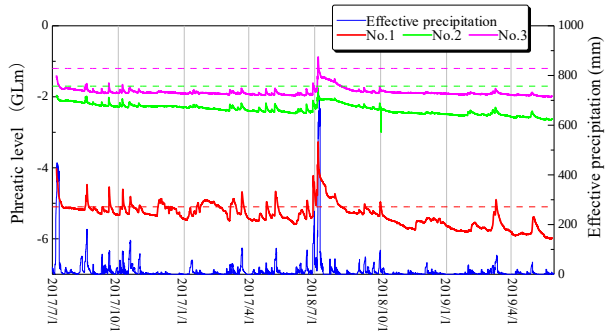

Figure 5 Water levels in observation wells and 24-hour effective precipitation

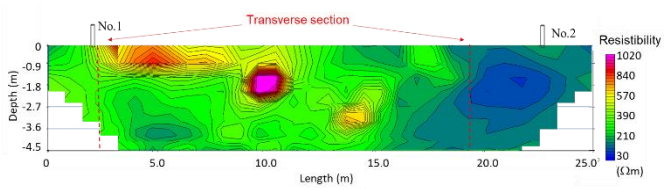

Figure 6 Electrical resistivity distribution on longitudinal embankment section

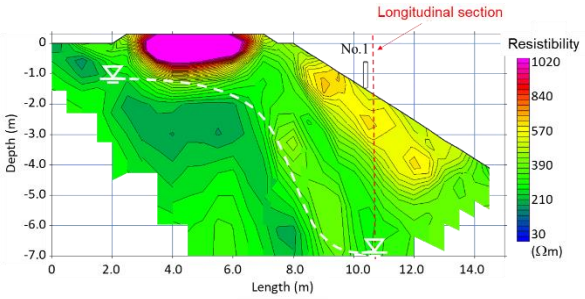

Figure 7 Electrical resistivity distribution on transverse embankment section (without drain pipe)

Figure 8 presents the electrical resistivity distribution determined for the drain pipe installation area. Drain pipes are indicated by black arrows in the figure. Figure 9 represents how the drain pipes drained water on the day of electrical prospecting. The drain pipes in the top row drained no water. In contrast, all drain pipes in the bottom row were observed to constantly drain water and are thought to have been useful for lowering the phreatic surface. The middle row was a mixture of pipes that drained and pipes that did not drain. Figure 8 shows phreatic levels measured in observation wells 2 and 3, along with white dashed lines indicating the position of the phreatic surface with electrical resistivity distribution taken into account. In summary, as the drainage condition suggests, most drain pipes in the bottom row and some drain pipes in the middle row were surmised to be below the phreatic surface. Thus, electrical prospecting can be valid for ascertaining the phreatic surface at the site, and the phreatic surface takes the form shown in Figure 8 owing to drain pipe installation.

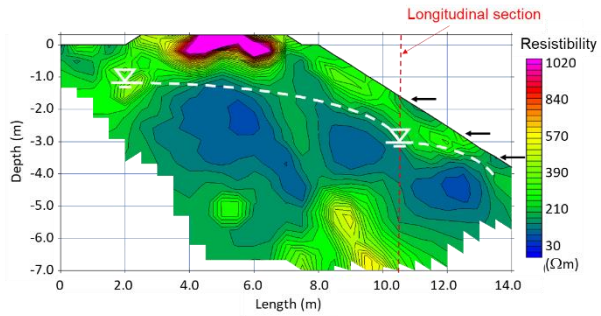

Figure 8 Electrical resistivity distribution on transverse embankment section (with drain pipe)

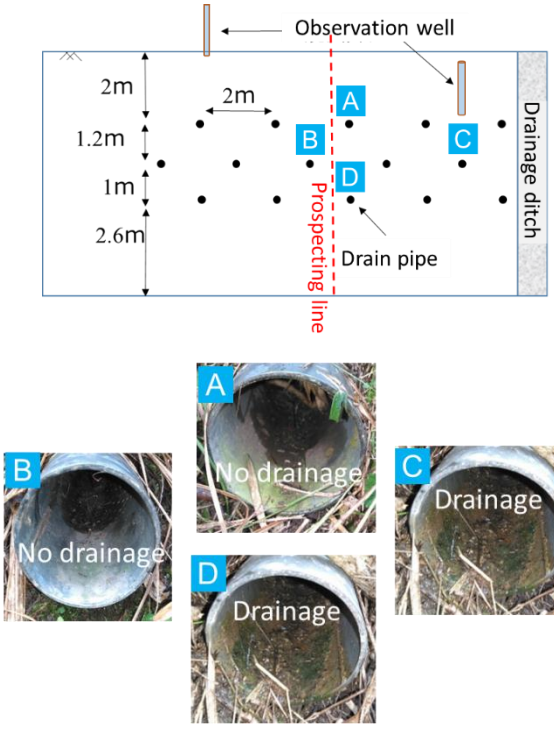

Figure 9 Drainage condition of drain pipes during prospecting

3. UNSATURATED SOIL/WATER COUPLED ANALYSIS WITH DRAIN PIPES TAKEN INTO ACCOUNT

For drain pipe installation planning to incorporate drainage effects of the installed pipes, it was necessary to perform an unsaturated soil/water coupled analysis.

3.1 Numerical Model

The analysis used the soil/water/air coupled finite element analysis code DACSAR-MP (Sugiyama et al., 2016). As a mathematical model, the constitutive unsaturated soil model proposed by Ohno et al. (2007) was used. Effective stress is given by the following equation.

$$\boldsymbol{\sigma}' = \boldsymbol{\sigma}^{net} + p_s \mathbf{1} \tag{1}$$

$$\boldsymbol{\sigma}^{net} = \boldsymbol{\sigma} - p_a \mathbf{1}, \; p_s = S_e s \tag{2}$$

$$s = p_a - p_w, \; S_e = \frac{S_r - S_{rc}}{1 - S_{rc}} \tag{3}$$

where, $\boldsymbol{\sigma}'$ is the effective stress tensor; $\boldsymbol{\sigma}^{net}$ is the net stress tensor; $\mathbf{1}$ is the unit tensor; $\boldsymbol{\sigma}$ is the total stress tensor; s is suction; p_s is the suction stress; p_a is the pore air pressure; p_w is the pore water pressure; S_r is the degree of saturation; S_e is the effective degree of saturation; and S_{rc} is the degree of residual saturation at $s \to \infty$. The constitutive relationship is given by the following equation.

$$\boldsymbol{\sigma}' = \mathbf{D} : \boldsymbol{\varepsilon} - \mathbf{C} \cdot \dot{S}_e \tag{4}$$

where, $\mathbf{D}$ is the elastoplastic rigidity matrix; $\boldsymbol{\varepsilon}$ is the strain tensor; and $\mathbf{C}$ is the tensor representing rigidity changes resulting from unsaturated conditions. As illustrated above, the effect of unsaturated conditions on deformation causes changes in effective stress and

rigidity. Continuity equations of pore water and pore air are given by the following equations.

$$n\dot{S}_r - S_r\dot{\varepsilon}_v + \mathrm{div}\tilde{\mathbf{v}}_\mathbf{w} = 0 \tag{5}$$

$$(1-S_r)\dot{\varepsilon}_v + n\dot{S}_r - n(1-S_r)\frac{\dot{p}_a}{p_a + p_0} - \mathrm{div}\tilde{\mathbf{v}}_\mathbf{a} = 0 \tag{6}$$

where, n is porosity; $\tilde{\mathbf{v}}_\mathbf{w}$ and $\tilde{\mathbf{v}}_\mathbf{a}$ are relative velocities of pore water and pore air, respectively; ε_v is volumetric strain; and p_0 is the atmospheric pressure. The specific hydraulic conductivity under unsaturated conditions relative to the saturated hydraulic conductivity was determined by Mualem's equation (1976) below.

$$k_{rw} = S_e^{1/2}\left[1-\left(1-S_e^{1/m}\right)^m\right]^2 \tag{7}$$

where, k_{rw} is the specific hydraulic conductivity and m is a shape function. Soil-water characteristic curves that represent the relationship between the degree of saturation and suction are known to differ between drying and wetting processes and to be suction history-dependent. The present study used the soil-water characteristic curve model proposed by Kawai et al. (2007), which modeled the influence of hysteresis. In the analysis code, the constitutive model and the continuity equations were coupled via effective stress and the soil/water characteristic curve model to simultaneously express deformation and seepage behaviors.

While in our previous studies head and flow rate boundaries were used as hydraulic boundary conditions, a permeable boundary was added to these conditions in this study. The permeable boundary is a hybrid boundary, which means that under positive suction conditions an unknown head is determined by calculation and under negative suction conditions (i.e., when the pore water pressure exceeds zero given that the air pressure equals the atmospheric pressure), the permeable boundary is automatically converted to a zero-suction drained boundary. Drain pipes are known to be ineffective at draining under unsaturated conditions, as proven by the results obtained by Saito et al. (1968) The effect of a drain pipe is expressed by setting up a permeable boundary at the position where the drain pipe is installed. Additionally, by setting up a permeable boundary along the embankment slope, it becomes possible to express the seepage that occurs when the phreatic surface reaches the slope.

3.2 Simulation of Boundary Phreatic Level Fluctuation

To verify the validity of expressing installed drain pipes as a permeable boundary, a simulation was conducted to model the embankment on which electrical prospecting was carried out. Figure 10 illustrates an analysis region and boundary conditions that simulate a transverse section of the embankment and its boundary conditions. The embankment was greatly subject to the influence of phreatic level fluctuation in the slope behind it. Therefore, a head boundary was set up at the left edge of the analysis region and permeable boundaries were set up along the embankment slope and where the drain pipes were installed. Table 1 shows soil parameters used in the analysis. Figure 11 shows soil-water characteristic curves. Because the soil conditions of the actual site were unknown, the analysis used parameters from similar embankment material obtained from a housing construction site. The analysis assumed post-compaction soil conditions; assigned a degree of saturation of 0.9 and suction of 1.5 kPa to all elements in the analysis region; and allowed the analysis region to stand for 10 days to reproduce initial conditions seen prior to the phreatic surface rising due to rainfall. Subsequently, to express infiltration of external water from behind the embankment, the left edge of the analysis region was given a total head corresponding to the increasing phreatic level. Thus, a change in the phreatic surface after rainfall was expressed. To represent the phreatic level on the day of electrical prospecting, this study used two water levels, namely, 5.6 m from the bottom and 6.1 m from the bottom (maximum water level), which were obtained by consulting relationships previously observed between effective precipitation and phreatic level.

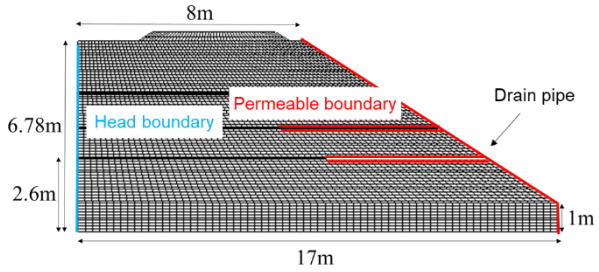

Figure 10 Transverse section analysis region and hydraulic boundary conditions

Table 1 Parameters used for analysis

λ	κ	M	m	n_E
0.087	0.009	1.375	0.6	1.0
a	n_s	S_{rc}	k_x	k_y
10.0	1.0	0.43	2.4×10^{-3}	2.4×10^{-3}

k_x, k_y :Saturated hydraulic conductivity in unit (m/day)

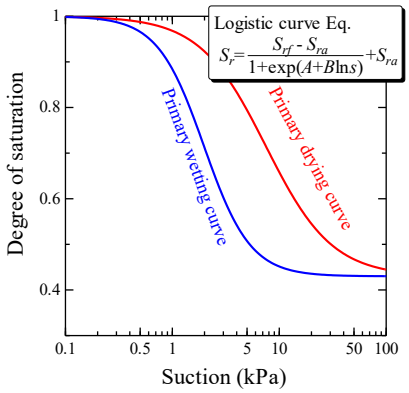

Figure 11 Soil-water characteristic curves used for analysis

Figure 12 illustrates the initial degree of saturation occurring before the rise of the phreatic surface in the transverse section analysis. From this state, the water level behind the embankment was allowed to rise to determine the phreatic surface in a condition without the drainage effect of drain pipes (with no permeable boundary assigned in the drain pipe area). Figures 13 and 14 present degree of saturation distributions in the cases of 5.6 m and 6.1 m water levels, respectively, assumed behind the embankment. In these figures, a pressure head of zero is shown with a white line, which can be construed as a phreatic surface formed in the embankment. The red dashed lines in the "After passage of two days" figures represent phreatic surfaces estimated based on the results of electrical prospecting. In both cases, the phreatic surface had reached the embankment slope two days later, indicating leaching out of the slope. The rise of the phreatic surface reached a steady state about one day after the rise in the water level behind the embankment. The phreatic surfaces shown in the "After passage of two days" figures are thought to represent a state in which the water balance in the embankment was in equilibrium. Naturally, seepage would occur in higher areas of the embankment slope in response to higher water levels in the ground behind the embankment. A 50 cm difference in the phreatic level behind the embankment led to a 20 to 25 cm difference in seepage location on the embankment slope. This would substantially affect the stability of the embankment.

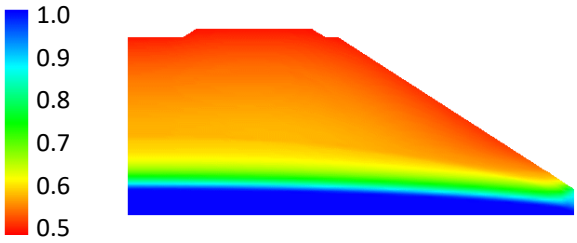

Figure 12 Initial degree of saturation distribution

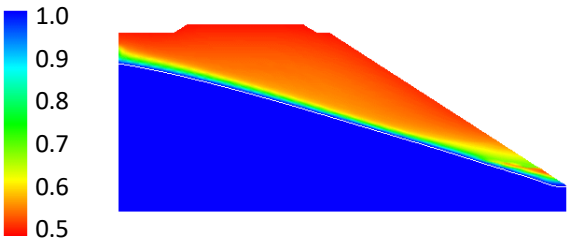

(a) After passage of 0.6 days

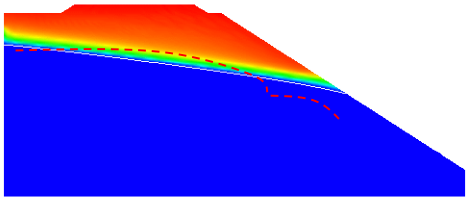

(b) After passage of two days

Figure 13 Degree of saturation distribution at 5.6 m water level in the ground behind the embankment

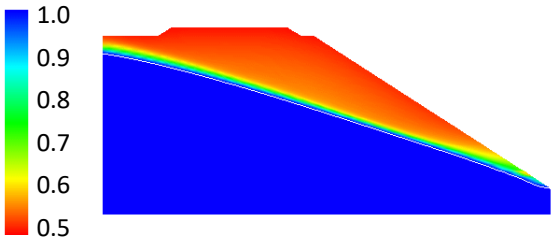

(a) After passage of 0.6 days

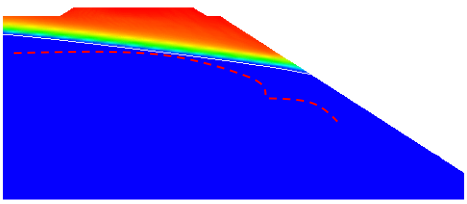

(b) After passage of two days

Figure 14 Degree of saturation distribution at 6.1m water level in the ground behind the embankment

Figure 15 shows the degree of saturation distribution two days later for the embankment with installed drain pipes in the case the water level was 5.6 m in the ground behind the embankment. In this figure, a white dashed line represents the phreatic surface location determined based on Figure 13 with no drain pipes. Figure 15 demonstrates that drain pipes prevented the phreatic surface from reaching the embankment slope. It also represents the form of the phreatic surface (red dashed line) determined by means of electrical prospecting. Generally, the electrical resistibility expresses soil moisture. Therefore, capillary zone, which shows saturated zone above the phreatic surface, tends to be tracked down by the electrical prospecting. This is because the phreatic surface obtained from simulation is located below one obtained from the electrical prospecting. Actually, identification of the phreatic surface by the electrical prospecting is dependent on the contour of electrical resistibility regarded as the value indicating saturation in Figure 8. It is expectable that we can track down the actual phreatic surface through comparing the electrical prospecting results with numerical simulations. Moreover, while a drain pipe exerts a three-dimensional effect, the figure expresses drain pipes under a plane strain condition, amplifying the drainage effect. The form of the phreatic surface suggests almost no effect for the top row of drain pipes. With three-dimensional effects taken into account, the actual phreatic surface is predicted to form between phreatic surfaces determined through transverse section analysis considering the absence and presence of drain pipes, as revealed by the actual phreatic surface indicated with the red dashed line. Figure 16 shows a degree of saturation distribution in the embankment with installed drain pipes, assuming a 6.1 m water level in the ground behind the embankment. Overall, the phreatic surface is high in this case. The top row of drain pipes also demonstrates drainage effects to some extent. However, the effect of the bottom row of drain pipes is dominant. Consequently, it is highly likely that drainage performance is overestimated by performing a simulation under a plane strain condition as described above. Therefore, an analysis was conducted along a longitudinal section of the embankment.

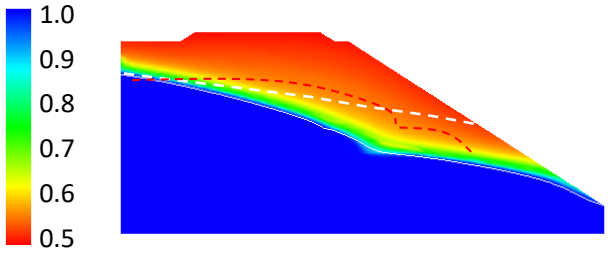

Figure 15 Degree of saturation distribution in embankment with drain pipes at 5.6 m water level in the ground behind the embankment

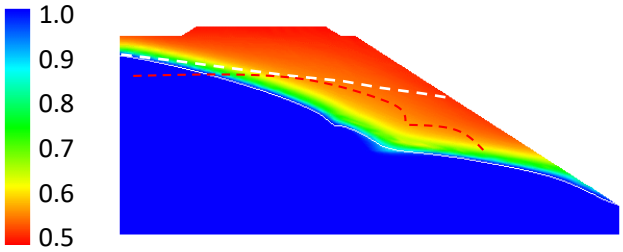

Figure 16 Degree of saturation distribution in embankment with drain pipes at 6.1 m water level in the ground behind the embankment

Figure 17 presents a volumetric strain distribution based on the results of coupled analysis. Volumetric compression is noticeable at the tip of the drain pipe, where the phreatic surface is projected to substantially drop due to the drain pipe effect. Above the volumetric compression, an expansion region is observed. This suggests the possibility of looseness occurring due to the lowered phreatic surface, which in turn was due to the installation of drain pipes. Note that this study uses only the application of a permeable boundary to express drain pipe performance and that it does not take into account the effect of enhanced restraint produced by driving steel pipes into the ground (steel pipes are highly rigid in comparison with the ground material). The deformation behavior identified in this study was induced by seepage and differs from actual behaviors. In the future it should become possible to take deformation stability into account by performing a coupled analysis using varying deformation parameters for the drain pipe area.

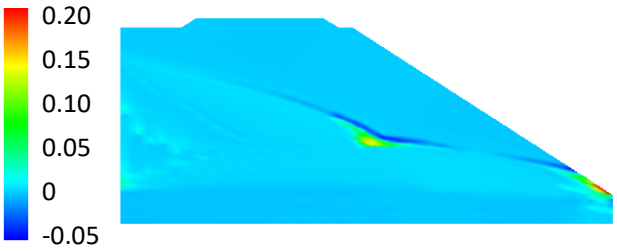

Figure 17 Volumetric strain distribution resulting from drain pipe installation at 5.6 m water level in the ground behind the embankment

3.3 Rainfall Seepage Simulation

As discussed previously, the effect of drain pipes is overestimated in transverse section analysis under a plane strain condition along the drain pipe's longitudinal direction. Given the three-dimensional form of a drain pipe, a three-dimensional analysis is required to ascertain the extent to which the draining effect reaches in the direction of the normal to the drain pipe's outer surface. However, because drain pipe size is small relative to the analysis region, a concern arises that an increasing number of elements used in the analysis may make the numerical computation complicated. This study, therefore, attempted to supplement the analysis with a simplified three-dimensional effect by setting an analysis region, as shown in Figure 18, and by additionally conducting an analysis of a longitudinal section of the embankment. This figure shows a permeable boundary applied at the elements indicated with red dots to express drain pipes. The right and left edges of the analysis region were assumed to be undrained boundaries, and the width of the analysis region was varied to analyze horizontal installation intervals of drain pipes and the effective drainage range. The analysis steps were performed as follows: first, to use uniform sets of initial conditions after element generation, a total head of 1.5 m was assigned to the bottom of the analysis region; then, after making sure a steady state had been reached, the bottom was transformed to a permeable boundary; and finally, the top was given a flow rate corresponding to a certain rainfall intensity for a seepage simulation.

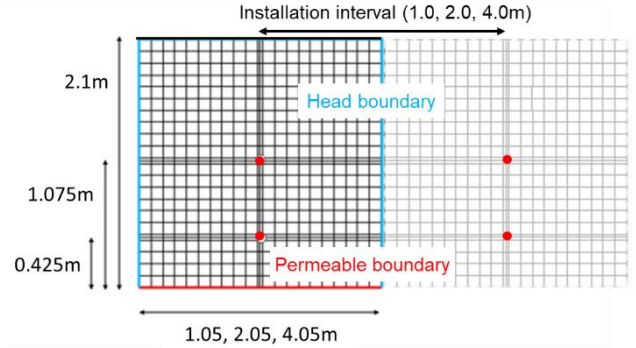

Figure 18 Longitudinal section analysis region and hydraulic boundary conditions

Figure 19 shows degree of saturation distributions observed for the horizontal installation interval of drain pipes at 1.0 m or 2.0 m, given a rainfall intensity of 30 mm/h after a steady state was reached. In the figure, white solid lines represent phreatic surfaces expressing zero pressure head. In both cases the phreatic surface was formed at or higher than the elevation of the lower drain pipe. At the installation interval of 2.0 m, the water level was higher at the location of the lower drain pipe. Figure 20 depicts the change of pressure head during rainfall duration with time at the lower left of the analysis region, with the aim of expressing the drainage capacity of drain pipes as their capacity to mitigate phreatic level rise against rainfall intensity. In each case, the water pressure decreased after the start of rainfall. The reason for this is that a water level of 1.5 m above the bottom was set as a pre-rainfall initial condition, and the bottom was subsequently transformed to a permeable boundary. More specifically, before the rainwater entering through the ground surface reached the phreatic surface and caused it to rise again, the phreatic level went down due to drainage through the bottom. The figure reveals that when infiltrated rainwater reached the phreatic surface, the phreatic level began to rise and that when the infiltrated rainwater was balanced with the drainage capacity of the drain pipes, the phreatic level became stable. All cases exhibited a high phreatic level in response to increases in rainfall intensity. Where the pressure head was around or higher than 1.0 m, the upper drain pipes were considered functional. Comparisons between these results reveal that at the rainfall intensity used in the analysis of installation intervals of 1.0 m, adequate drainage performance was projected from the lower drain pipes alone. Where the pressure head was higher than 1.0 m, drainage depended on the drainage capacity of the upper drain pipe. In this context, the pressure head is regarded as the water level at the point of the highest phreatic surface at the center of horizontally arranged drain pipes. Thus, through these analyses, it should be possible to predict the amount of rise of the phreatic surface resulting from a certain assumed rainfall intensity with respect to different pipe installation intervals and to estimate, in the design phase, suitable installation intervals and the required number of drain pipes in a vertical direction.

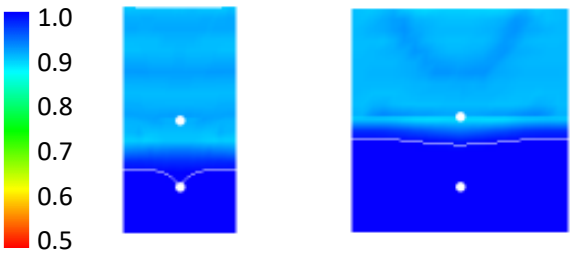

(a) Installation interval 1.0 m (b) Installation interval 2.0 m

Figure 19 Degree of saturation distribution in embankment revealed by longitudinal section analysis

Additionally, the previously analyzed transverse sections of the embankment were also used to conduct a rainfall simulation. The analysis region conformed to that shown in Figure 9. To examine the behavior of the side of the embankment at the greatest risk of failure, the analysis region was allowed to stand for two days with a phreatic level of 6.1 m assigned to the left edge of the analysis region. Subsequently, the top and slope were given a flow rate corresponding to a certain rainfall intensity. For this step, the rainfall intensity in the slope area was multiplied by the cosine of the slope angle. The rainfall duration was set to 3 h, which was followed by allowing the analysis region to be left as it is while analyzing the lowering of the phreatic surface after the termination of the rainfall. Figure 21 gives a degree of saturation distribution observed 1 h after the end of the rainfall. The distribution was obtained by a seepage analysis of the transverse section. In the figure, white solid lines represent phreatic surfaces determined through the analysis. Rainwater infiltrated through the top of the region flowed downward in a vertical direction. In contrast, rainwater infiltrated through the slope tended to be guided and flow downward in a direction parallel to the slope and toward the toe of the slope. The reason for these observations is that, as illustrated by Equation (7), the unsaturated hydraulic conductivity was a function of the degree of saturation and that the water tended to selectively flow through the high hydraulic conductivity zone close to the slope, in which the degree of saturation increased. As a result, for a short period of time, infiltrated rainwater did not contribute to the rise of the phreatic surface deep in the embankment, a location where the effect of the phreatic level behind the embankment was dominant. Differences arising from different levels of rainfall intensity are manifest at the tip of the lower drain pipe and in the zone proximal to the pipe's outlet on the slope.

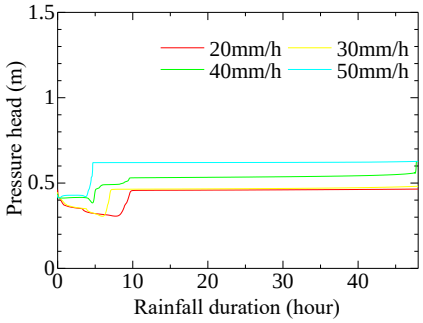

(a) Installation interval 1.0 m

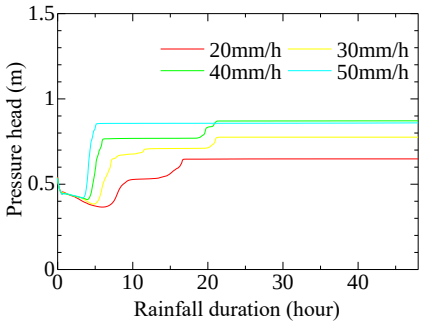

(b) Installation interval 2.0 m

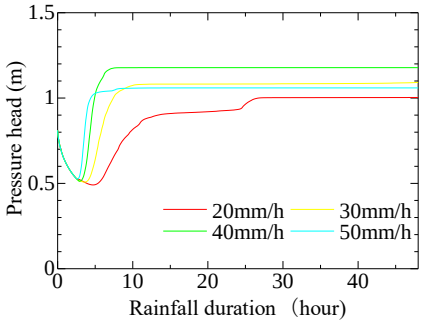

(c) Installation interval 4.0 m

Figure 20 Pressure head changes at lower left longitudinal section analysis region

For a comparison between quantitative effects of drain pipes, as in the case of the analysis of the longitudinal section, Figure 22 shows changes in pressure head obtained at the lower edge of the boundary at the outlet of the lower drain pipe. The figure reveals increases in water pressure starting from the beginning of precipitation with respect to all levels of rainfall intensity. Under high rainfall intensity conditions, the water level continued to rise for some time after the termination of rainfall. This indicates that, after the termination of rainfall, the infiltrated rainwater reached the phreatic surface and caused the phreatic surface to rise. Because subsequent behavior of decreasing water pressure depended on the total quantity of rainwater that had infiltrated by the end of rainfall, the lowering of the phreatic surface attributable to drainage diminished with increasing rainfall intensity. At the rainfall intensity of 50 mm/h, the length of the lower drain pipe up to the slope stayed below the phreatic surface, and, as a result, the water pressure remained at a constant value, as verified in Figure 21.

Safety factors with respect to slope failure greatly vary with phreatic surface position. Furthermore, learning about the phreatic surface is critical for the study of failure due to the earth piping. It is highly probable that, for a drain pipe installation area, the phreatic surface position can be computed in a simplified way and be incorporated in drain pipe installation design by (1) assuming that a transverse section analysis can determine the lowest phreatic surface position, and then by (2) adding to this position the maximum rise increment of the phreatic surface above the drain pipe position, as determined through a longitudinal section analysis, for each drain pipe interval.

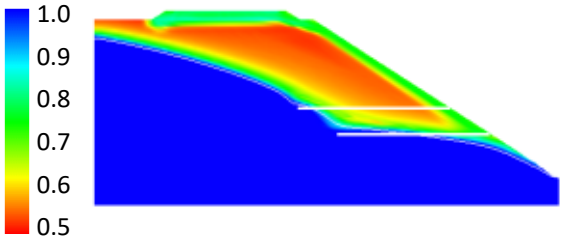

(a) Rainfall intensity 20 mm/h

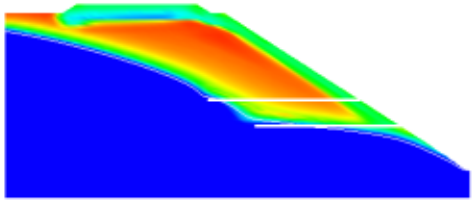

(b) Rainfall intensity 30 mm/h

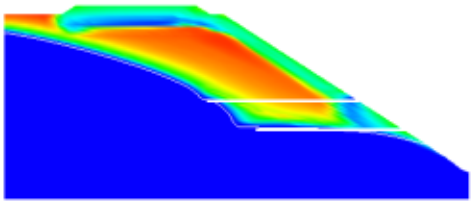

(c) Rainfall intensity 40 mm/h

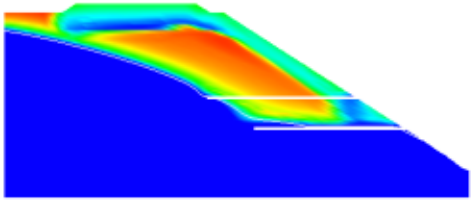

(d) Rainfall intensity 50 mm/h

Figure 21 Degree of saturation distribution revealed by transverse section rainfall analysis

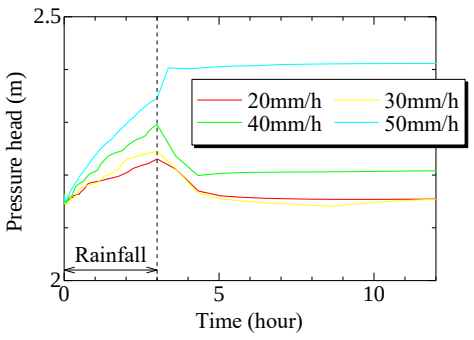

Figure 22 Pressure head changes on bottom right below lower drain pipe

4. CONCLUSIONS

This study explored a technique of quantitatively predicting phreatic surface positions by expressing the drainage performance of drain pipes in a numerical analysis, producing the following results.

(1) The position and form of the phreatic surface was determined by means of electrical prospecting for an embankment with

installed drain pipes, and the effects of drain pipes were visualized.

(2) Drainage performance can be verified in the framework of common unsaturated seepage analysis by setting up a permeable boundary in the drain pipe installation area. Moreover, because a soil/water/air coupled analysis makes deformation analyses possible, by taking into account rigidity changes arising from drain pipe installation, future research tasks can include studying the effectiveness of drain pipes in improving the stability and other properties of embankments.

(3) We proposed a technique of combining transverse and longitudinal section analyses of embankment usable to express the three-dimensional drainage effects of drain pipes. A transverse section analysis alone overestimates drainage performance. This drawback can be complemented by determining the elevation of the formed phreatic surface above the drain pipe position through a longitudinal section analysis. At the same time, the rising trends of the phreatic surface, varying with the horizontal installation intervals of drain pipes and corresponding to rainfall intensity, can be simulated for a comparative study.

(4) By analyzing seepage while faithfully reproducing actual topographic and soil conditions in a numerical analysis, it potentially becomes possible to explore suitable and efficient drain pipe arrangements and the lengths of drain pipes driven into the ground.

5. REFERENCES

Cai, F., Ugai, K., Wakai, A., and Li, Q. (1998) "Effects of horizontal drains on slope stability under rainfall by three-dimensional finite element analysis," Computers and Geotechnics, 23, Issue 4, pp255-275.

Chen, C. N., and Chen H. Y. (2013) "Distributions of pore water pressure surround a horizontal drain pipe on a retaining wall under steady state condition," Journal of Mechanics, 29, Issue 2, pp263-272.

Choi, E. C. C. (1983) "Seepage around horizontal drains in hill slopes," Journal of Hydraulic Engineering, 109, Issue 10, pp1363-1368.

Fujii, M., Okada, K., Sugiyama, T., Muraishi, H., Samizo, M., and Kusano, K. (1996) "Experiment toinfluence of interval of drainpipes," Proceedings of JGS the 31st Annual Meeting, pp1999-2000 (in Japanese).

Kawai, K., Iizuka, A., Hayakawa, E., and Wang, W. (2007) "Non-uniform settlement of compacted earth structures caused by the deformation characteristics of unsaturated soil on wetting," Soils and Foundations, 47, Issue 2, pp195-206.

Kitaguchi, S., Tokida, K., Linh, V. H., Akita, T., Yoshikai, Y., and Kamide, S. (2013) "Study on drainage function and its estimation of drain pipe," Proceedings of the Kansai Geo-Symposium 2017, pp197-202.

Mualem, Y. (1976) "A new model for predicting the hydraulic conductivity of unsaturated porous media," Water Resources Research, 12, Issue.3, pp514-522.

Ohno, S., Kawai, K., and Tachibana, S. (2007) "Elasto-plastic constitutive model for unsaturated soil applied effective degree of saturation as a parameter expressing stiffness," Journal of JSCE, C-63, Issue 4, pp1132-1141 (in Japanese).

Ota, N., Sugiyama, T., Watanabe, S., Kouma, T., Nishida, M., and Ishikawa, S. (2012) "Seepage analysis model for the drainage pipe applied to embankment," Railway Technical Research Report, 26, Issue 9, pp35-40 (in Japanese).

Rahrdjo, H., Hritzuk, K. J., Leong, E. C., and Rezaur, R. B. (2003) "Effectiveness of horizontal drains for slope stability," Engineering Geology, 69, Issue 3-4, pp295-308.

Rahardjo, H., Santoso, V. A., Leong, E. C., Ng, Y. S., and Hua, C. J. (2011) "Performance of horizontal drains in residual soil slopes," Soils and Foundations, 51, Issue 3, pp437-447.

Resnick, G. S., and Znidarčić, D. (1994) "Centrifugal modeling of drains for slope stabilization," Journal of Geotechnical Engineering, 116, Issue 11, pp1607-1624.

Saito, M., Uesawa, H., Menjo, S., and Yasuda, Y. (1968) "Effect of drainage for stability of embankment slopes by perforated pipes on the New Tokaido Line," Railway Technical Research Report, 631, pp1-18 (in Japanese).

Singh, J., Horikoshi, K., Mochida, Y., and Takahashi, A. (2019) "Centrifugal tests on minimization of flood-induced deformation of levees by steel drainage pipes," Soils and Foundations, 59, Issue 2. pp367-379.

Sugiyama, Y., Kawai, K., and Iizuka, A. (2016) "Effects of stress conditions on B-value measurement," Soil and Foundations, 56, Issue 5, pp848-860.

Watanabe, S., Ota, N., Nishida, M., and Asano, Y. (2015) "Nomogram for the executions specification of drain pipes for earthfills," Railway Technical Research Report, 29, Issue 1, pp29-34 (in Japanese).